molecular pharmaceutics

ACS AuthorChoice

Article

pubs.acs.org/molecularpharmaceutics

Terms of Use

Rapid Measurement of Intracellular Unbound Drug Concentrations

André Mateus,[†,‡] Pär Matsson,[†,§] and Per Artursson*[,†,§]

[†]Department of Pharmacy, Uppsala University, Box 580, SE-751 23 Uppsala, Sweden

[‡]Research Institute for Medicines and Pharmaceutical Sciences (iMed.UL), Faculty of Pharmacy, University of Lisbon, 1649-003 Lisbon, Portugal

[§]Uppsala University Drug Optimization and Pharmaceutical Profiling Platform (UDOPP)—a node of the Chemical Biology Consortium Sweden (CBCS), Department of Pharmacy, Uppsala University, 751 23 Uppsala, Sweden

Supporting Information

ABSTRACT: Intracellular unbound drug concentrations determine affinity to targets in the cell interior. However, due to difficulties in measuring them, they are often overlooked in pharmacology. Here we present a simple experimental technique for the determination of unbound intracellular drug concentrations in cultured cells that is based on parallel measurements of cellular drug binding and steady-state intracellular drug concentrations. Binding in HEK293 cells was highly correlated with binding in liver-derived systems, whereas binding in plasma did not compare well with cellular binding. Compound lipophilicity increased drug binding, while negative charge and aromatic functional groups decreased binding. Intracellular accumulation of unbound drug was consistent with pH-dependent subcellular sequestration, as confirmed by modeling and by inhibition of subcellular pH gradients. The approach developed here can be used to measure intracellular unbound drug concentrations in more complex systems, for example, cell lines with controlled expression of transporters and enzymes or primary cells.

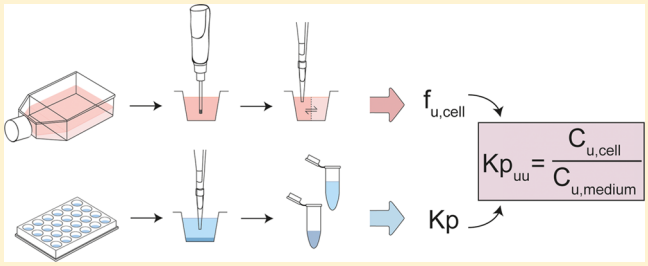

KEYWORDS: *intracellular unbound concentrations, drug binding, drug transport, drug accumulation, membrane partitioning*

INTRODUCTION

Approximately half of all known drug targets, and virtually all key drug metabolizing enzymes, are located in the cell interior.[1] Therefore, accurate determination of intracellular exposure to new drugs is paramount for the successful prediction of their pharmacokinetic, pharmacological, and toxicological profiles. The unbound drug concentration is particularly important, because it is generally considered to be the pharmacologically relevant concentration. Traditionally, the intracellular unbound drug concentration has been equated with that in plasma.[2,3] However, transport proteins that mediate the flux of drugs, metabolites, and endogenous compounds across cellular membranes can result in intracellular levels of substrate drugs markedly different from the levels in the extracellular environment (e.g., in the plasma). For instance, in suspended hepatocytes, uptake transporters may increase intracellular unbound concentrations of some substrates up to 500-fold compared to the extracellular medium.[4−7] However, additional cellular processes such as active efflux and metabolism might lead to lower ratios *in vivo*. Hence, a better understanding of the factors that determine intracellular unbound-drug exposure has the potential to considerably improve predictions of drug−drug interactions, intracellular efficacy, and adverse events.

Commonly applied methodologies to assess intracellular drug concentrations have various limitations. Either they do not distinguish between total and unbound drug,[8,9] they rely on nonphysiological assumptions (e.g., that membrane transport in hepatocytes occurs exclusively via passive diffusion[10,11]), or they employ nonphysiological conditions (e.g., use of incapacitated hepatocytes[12]). A more sophisticated approach derives intracellular unbound concentrations by mechanistic modeling but is limited by the need for experimentally demanding measurements at multiple time points and concentrations.[5−7] Thus, generic and reliable methods that rapidly measure and predict intracellular drug binding and unbound drug concentrations are clearly warranted.

In this work, we present a straightforward experimental technique for rapid determination of unbound intracellular drug concentrations through the combination of intracellular drug binding and steady-state intracellular total drug concentration measurements (Figure 1). We applied this technique to measure binding and accumulation of the unbound quantities of 30 physicochemically diverse compounds in cultured, human embryonic-kidney 293 cells (HEK293). Because of its negligible expression of transport proteins and drug-metabolizing enzymes,[13] the HEK293 cell line allows the study of intracellular binding and partitioning without these confound-

Received: February 13, 2013
Revised: April 26, 2013
Accepted: April 30, 2013
Published: April 30, 2013

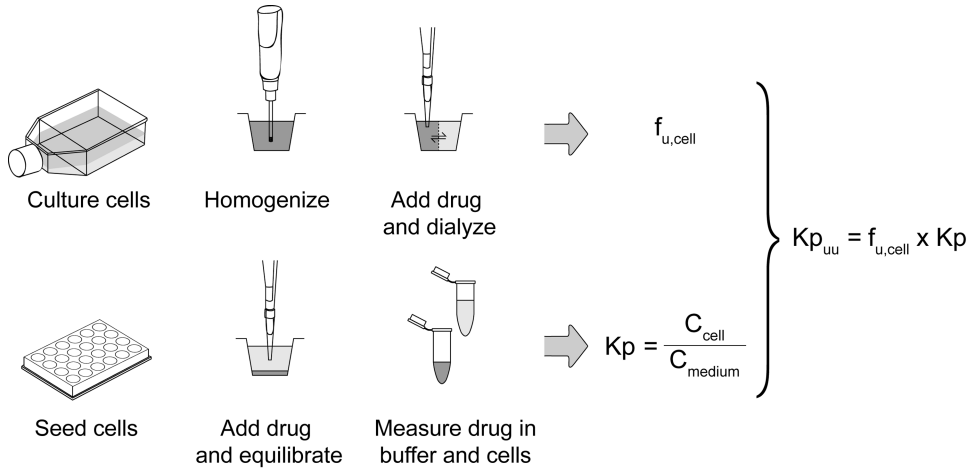

Figure 1. Determination of intracellular unbound drug accumulation ratio (Kp_{uu}) from intracellular binding ($f_{u,cell}$) and steady-state cellular uptake (Kp) measurements.

ing factors. We show that our methodology can be successfully used to obtain unbound drug concentrations in cultured cells and that binding in this simplistic cell model compares well with measurements in systems derived from liver. Because intracellular binding and accumulation are measured in separate experiments instead of deriving both parameters from the same data, no assumptions of passive membrane permeability and negligible metabolism are necessary. Consequently, the approach is readily extendable to cell lines with controlled expression of drug transporters and drug-metabolizing enzymes, as well as to more complex primary-cell models.

EXPERIMENTAL SECTION

Materials. All cell culture media and reagents were from Invitrogen (Carlsbad, CA) or Sigma-Aldrich (St. Louis, MO). Drug compounds were obtained from Abbott Laboratories (Sweden), Sigma-Aldrich (St. Louis, MO), Toronto Research Chemicals (Toronto, Canada), and OChem Inc. (Chicago, IL). All compounds were of analytical grade (≥95% purity). Stock solutions of compounds were prepared at a concentration of 10 mM in dimethyl sulfoxide (DMSO) and stored at −20 °C.

Cell Culture and Preparation of Experiments. Human embryonic kidney cells Flp-In-293 (HEK293) transfected with pOG44 and empty pcDNA5/FRT vectors (Invitrogen, Carlsbad, CA) were used throughout the study.[14] The cells were maintained in Dulbecco's modified Eagle's medium (DMEM) supplemented with 10% fetal bovine serum (FBS), 2 mM L-glutamate, and 75 μg/mL Hygromycin B, at 37 °C in a humidified 5% CO_2 atmosphere. Cells were used for a maximum of 25 passages after the establishment of stable, empty vector transfectants.

For measurements of drug binding, cells were harvested from T75 flasks using 0.05% trypsin, then centrifuged at 260 × *g* for 5 min. Cells were thereafter washed once with Dulbecco's phosphate-buffered saline, counted using a NucleoCounter NC-100 (Chemometec, Allerød, Denmark), and centrifuged again at 260 × *g* for 5 min. The supernatant was discarded, and the cell pellet was stored at −20 °C pending preparation of the cell homogenate.

For cellular uptake experiments, cells were seeded at a density of 600 000 cells/well in CellBIND 24-well plates (Corning, Amsterdam, Netherlands) and grown for approximately 2.5 days in DMEM (without phenol red) supplemented with 10% FBS and 2 mM L-glutamate.

Thawing and Preparation of Cryopreserved Human Hepatocytes. Liver tissue was obtained from human donors undergoing surgical liver resection at the Uppsala University Hospital (Sweden) upon informed consent, as approved by the Uppsala Regional Ethical Review Board (ethical approval no. 2009/028). Hepatocytes were isolated by a two-step collagenase perfusion method, as previously described,[15] and cryopreserved.[16]

On the day of the experiments, cryopreserved human hepatocytes were thawed at 37 °C, transferred into approximately 50 mL of Hank's buffered salt solution (HBSS), and centrifuged at 100 × *g* for 10 min. The cells were then suspended in HBSS and counted. After a second identical centrifugation step, the cell pellet was used immediately for the measurement of drug binding as described below.

Measurements of Intracellular Drug Binding. Compound binding to intracellular structures was measured through equilibrium dialysis of cell homogenate. The homogenate was prepared by suspending a pellet of HEK293 cells or human hepatocytes (prepared as described above) in HBSS to a concentration of 10 × 10^6 cells/mL. The suspension was then homogenized for 10 s with a VCX-500 ultrasonic processor (Sonics & Materials, Newton, CT) at 20% intensity.

A subset of nine compounds (astemizole, caffeine, candesartan, diltiazem, lovastatin, metoprolol, ondansetron, repaglinide, simvastatin acid) covering the ranges of lipophilicity and charge states in the complete compound set (n = 30) was used to assess binding to human hepatocyte homogenate at a compound concentration of 0.1 μM and to determine the concentration dependence of binding to HEK293 cell homogenate. For the latter, compounds were added to the homogenate to give final concentrations of 0.01, 0.1, 1, 10, and 100 μM, with the exception of simvastatin acid for which the lowest concentration was excluded due to analytical limitations.

Samples were dialyzed using a Rapid Equilibrium Dialysis device (Thermo Fisher Scientific Inc., Rockford, IL) by transferring 200 μL of compound-spiked homogenate to one chamber of the dialysis unit (homogenate chamber) and 350 μL of HBSS to the other chamber (buffer chamber). The

dialysis unit was incubated at 37 °C and 900 rpm on an orbital shaker for 4 h. Compound stability in the homogenate was evaluated using two separate approaches: first, compound-spiked homogenate was incubated in wells without a dialysis membrane under the same conditions as the dialysis samples. Concentrations at the end of the experiment were compared with those in identical control samples kept at 4 °C. Second, mass balances were calculated at the end of all dialysis experiments. For all compounds, their concentrations after incubation at 37 °C were within ±15% of the 4 °C controls. Similarly, mass balances were consistently >80%.

At the end of the incubation, 20 μL of each sample from the homogenate and buffer chambers was transferred to a 96-well plate. Blank buffer or blank homogenate (20 μL) was added to the samples from the homogenate or buffer chambers, respectively, to yield identical matrices. Protein was precipitated by adding 160 μL of IS solution [50 nM warfarin (internal standard) in acetonitrile:water (60:40)] to all samples and centrifuging for 20 min at 2465 × *g*. After centrifugation, the compound concentration in the supernatant was quantified using UPLC-MS/MS, as described in the Analytical Procedures section.

Cell binding for the complete set of compounds was determined at a concentration of 0.1 μM, with the exception of nelfinavir and lopinavir which, due to their low water solubility, were determined at 0.01 μM. The unbound drug fraction in the cell homogenate ($f_{u,hom}$) was calculated according to:

$$f_{u,hom} = \frac{C_{buffer}}{C_{hom}} \quad (1)$$

where C_{buffer} is the compound concentration in the buffer chamber and C_{hom} is the compound concentration in the homogenate chamber. The unbound drug fraction in the cell ($f_{u,cell}$) was calculated after correcting for homogenate dilution (D)[17] according to:

$$f_{u,cell} = \frac{1}{D\cdot(1/f_{u,hom} - 1) + 1} \quad (2)$$

D was estimated to be 70 for a 10 × 10^6 cells/ml cell suspension of HEK293 cells by assuming a spherical shape of cells in suspension with a cell diameter of 13.9 ± 0.13 μm. For primary human hepatocytes, D was estimated to be 45, based on a diameter of 16.2 ± 0.37 μm. The cell diameters were determined by optical microscopy for a total of 180 cells on three independent occasions. The unbound fraction of each compound was measured in 3−5 independent experiments.

Measurements of Intracellular Drug Accumulation. Steady-state cellular uptake was measured in mock-transfected HEK293 cells seeded in 24-well plates (as described in the Cell Culture and Preparation of Experiments section). Compound solutions were prepared in HBSS from DMSO stock solutions to a final concentration of 0.1 μM (resulting in DMSO concentrations of 0.01% v/v). Before the experiment, cells were washed twice with prewarmed (37 °C) HBSS. Transport was initiated by the addition of 200 μL of compound solution, followed by incubation at 37 °C on an orbital shaker (300 rpm). Uptake was stopped after 45 min (separate experiments verified that this incubation time was sufficient to reach equilibrium; data not shown) by removing the incubated solutions of compound (medium samples) and washing the cells twice with ice-cold phosphate-buffered saline pH 7.4 (PBS) to remove any drug not associated with the cells. The cells were lysed for 15 min to extract the intracellular compound by adding 200 μL of IS solution. The medium samples were diluted 10 times with the same solution. The lysates and the diluted medium samples were transferred to a 96-well plate and centrifuged for 20 min at 2465 × *g*, and the compound was quantified in the supernatant as described in the Analytical Procedures section. Protein concentration was measured using the BCA Protein Assay Reagent Kit (Pierce Biotechnology, Rockford, IL) according to the manufacturer's instructions and determined in six representative wells per plate (one per column of the 24-well plate), in which the cells were incubated with the test compound but not lysed with IS solution, due to incompatibility of the BCA assay with the organic solvent used for compound extraction. Consistency in the amount of protein across wells was demonstrated in separate experiments (intraplate CV <10% across all wells of four plates, data not shown).

To assess the impact of changes in lysosomal pH, the steady-state cellular uptake of six compounds (three weak acids—diclofenac, indomethacin, and simvastatin acid—and three weak bases—diltiazem, propranolol, and verapamil) was measured in the presence of chloroquine at different concentrations (0−50 μM, representing an expected lysosomal pH range from 4.8 to 6.2).[18]

The ratio between total compound concentration in the cells and compound concentration in the medium (Kp) at any time point or concentration was calculated according to:

$$Kp = \frac{A_{cell}/V_{cell}}{C_{medium}} \quad (3)$$

where A_{cell} is the amount of compound in the cell lysate, V_{cell} is the HEK293 cell volume (6.5 μL/mg protein),[19] and C_{medium} is the compound concentration in the medium sample after correcting for sample dilution. All experiments were performed in triplicate on 3−5 independent occasions.

Determination of Unbound Drug Accumulation Ratios (Kp_{uu}). The unbound drug accumulation ratio (Kp_{uu}; Figure 1) was calculated according to:

$$Kp_{uu} = \frac{C_{u,cell}}{C_{u,medium}} = \frac{f_{u,cell}}{f_{u,medium}} \times Kp \quad (4)$$

where $C_{u,cell}$ is unbound intracellular concentration ($C_{u,cell} = f_{u,cell} \times C_{cell}$) and $C_{u,medium}$ is the unbound concentration in medium ($C_{u,medium} = f_{u,medium} \times C_{medium}$). Binding in the medium was considered to be negligible (i.e., $f_{u,medium} = 1$).

Analytical Procedures. Compounds were quantified using a Waters Xevo TQ MS with electrospray ionization coupled to an Acquity UPLC system (Waters, Milford, MA). Separation was done on a Waters BEH C18 column, 2.1 × 50 mm (1.7 μm), at 60 °C over a 2 min gradient with a flow rate of 0.5 mL/min. Solvent A consisted of 5% acetonitrile and 0.1% formic acid in water, and solvent B consisted of 0.1% formic acid in acetonitrile. The chromatographic run comprised a linear gradient from 0.5 to 1.2 min starting at 5% of solvent B and ending at 90%, followed by a hold from 1.2 to 1.6 min and a linear gradient to return to the initial conditions at 1.7 min. For caffeine and metoprolol, due to their high polarity, the initial conditions were 1% of solvent B. Samples were kept at 10 °C until injection. The mass transitions and their respective cone voltages and collision energies can be found in Table S1 of the Supporting Information.

Table 1. Physicochemical Characteristics of the Compound Set[a]

molecular charge at pH 7.4	n	log P[b]	log $D_{7.4}$[b]	molecular weight[b]	PSA[b]
negative	13	3.7 ± 0.4 (0.6−6.7)	1.3 ± 0.3 (−0.6 to 3.2)	442 ± 22 (296−559)	99 ± 8 (49−162)
neutral	9	3.3 ± 0.6 (−0.1 to 4.7)	3.2 ± 0.6 (−0.1 to 4.7)	488 ± 60 (194−721)	98 ± 14 (50−167)
positive	7	4.0 ± 0.5 (2.0−5.9)	2.7 ± 0.7 (0.1−5.2)	389 ± 47 (259−589)	54 ± 12 (6.5−114)
zwitterion	1	3.0 (n.a.)	3.0 (n.a.)	502 (n.a.)	81 (n.a.)

[a]Data are presented as the mean ± SEM, with the range in parentheses. [b]Calculated using ADMET Predictor (Simulations Plus, Lancaster, CA).

Molecular Descriptor Generation. Three-dimensional molecular structures were generated from SMILES representations using Corina, version 3.46 (Molecular Networks, Erlangen, Germany), keeping the lowest energy conformation of a maximum of 100 alternative ring conformations. The structures were used as input for molecular descriptor calculation with Dragon 6 (Talete, Milan, Italy) and ADMET Predictor, version 6.0 (SimulationsPlus, Lancaster, CA). A selection of >500 descriptors related to molecular size, shape, flexibility, lipophilicity, polarity, and charge, which have previously been used to describe ADME properties,[20−23] were included in the initial descriptor set. After removal of replicate molecular descriptors, descriptors having zero variance, and highly intercorrelated (r^2 > 0.85) descriptors, 84 descriptors remained (Table S3) and were used as the starting point for structure−activity model development.

Structure-Binding Modeling. Partial least-squares (PLS) projection was used to develop computational models for predicting drug binding from calculated molecular descriptors. A double-loop cross-validation (CV) procedure was used to provide an unbiased estimate of the prediction accuracy;[23,24] the data set was first randomly divided into 10 outer-loop CV segments. In turn, each of these segments was used as hold-out prediction sets, while the compounds in the remaining nine segments were used for model training. The training data was further divided into 10 inner-loop cross-validation segments, and the inner loop was used to optimize model parameters and variable selection. The best model from the inner-loop optimization was then used to predict the outer-loop test set. Since all model optimization is performed in the inner loop, CV predictions in the outer loop represent an unbiased estimate of the true external model predictivity. Variable selection was performed in two phases: first, the descriptors with lowest absolute PLS weight were iteratively removed until only the 25 most important ones remained; second, the same procedure was repeated, but descriptors were reintroduced in the model if removal resulted in an inferior model. The entire double-loop procedure was repeated 100 times for different random partitionings of the data set to calculate confidence intervals of prediction accuracy estimates and model parameters. A permutation procedure was used to assess the statistical significance of the final models: the order of the dependent variable was randomly shuffled 10 000 times, and the predictions of the permuted data sets were compared to those for the original data set. All models gave predictions (as assessed by the root mean squared error of prediction; RMSE) well outside the range of background probabilities from the randomized data sets (permutation p < 0.0001).

Modeling of pH-Dependent Unbound Drug Accumulation. For comparison purposes, a reference model of intracellular unbound drug accumulation was derived based on pH partitioning theory.[25] The model included three compartments: the extracellular medium (with a volume of 200 μL and a pH of 7.4, as described in the Measurements of Intracellular Drug Accumulation section), the cytosol (considered to have a pH of 7.1[26] and a volume of 6.5 μL/mg protein[19] [i.e., corresponding to an average total cytosolic volume of 2.2 μL per well, based on an average protein content of 0.34 ± 0.06 mg/well]), and the endolysosomal space (assumed to have a pH of 4.8[27] and 0.82% of the cytosolic volume[28]). Compound transfer between the three compartments was limited to the unbound fraction of the un-ionized molecular species (see schematic drawing in Figure 5B). Hence, unbound equilibrium concentrations of the uncharged species ($C_{u,uncharged}$) were assumed to be equal in the three compartments. The concentrations of the charged species ($C_{u,charged}$) in each compartment were calculated from the Henderson−Hasselbalch equation on the basis of the compartment pH, the compound pK_a (for acids; pK_b for bases), and the concentration of the uncharged species:

$$C_{u,charged} = \frac{C_{u,uncharged}}{10^{(pK_a \text{ or } pK_b) - pH}} \quad (5)$$

Extensions were included in the model for compounds with multiple relevant pK_a or pK_b values.

The abundance of each species was calculated from the concentrations and respective compartment volumes, and these were used to obtain a predicted ratio between unbound concentrations in cell and in medium ($Kp_{uu,pred}$):

$$Kp_{uu,pred} = \frac{A_{u,cell}/V_{cell}}{A_{u,medium}/V_{medium}} \quad (6)$$

where A_u is the sum of the amounts of all the unbound species in the respective compartments and V is the compartment volume, with the "cell" compartment being the sum of the cytosolic and endolysosomal compartments.

Statistics. All results are presented as the mean ± standard error of the mean (S.E.M.), unless otherwise stated. The Wilcoxon rank test was used to assess statistical significance of comparisons of two groups and the Kruskal−Wallis test for comparisons of multiple groups.

RESULTS

Compound Selection. The 30 drugs and drug-like compounds included in this study were chosen to cover a wide range of key physicochemical properties, including lipophilicity, molecular weight, and charge state. The majority of the compounds (67%) overlap with other studies assessing unbound intracellular concentrations.[5−7,10−12] Notably, these used different methodologies, enabling comparisons between the approaches. With future studies in mind, 12 of the compounds were included because they were previously reported to be OATP1B1 substrates.[29] These and other compounds reported to be substrates of transport proteins were considered to be passively transported in the HEK293 cells, on the basis of expression results,[13] and functional studies using transporter substrates (data not shown), indicating the

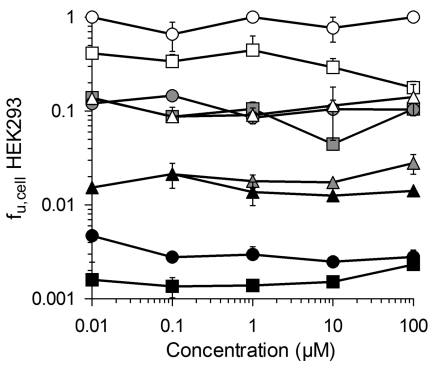

	Compound	log $D_{pH\,7.4}$	Charge
△	Candesartan	-0.11	–
▲	Simvastatin acid	1.74	–
▲	Repaglinide	3.22	–
○	Caffeine	-0.64	n
●	Ondansetron	2.05	n
●	Lovastatin	4.49	n
□	Metoprolol	0.05	+
■	Diltiazem	2.93	+
■	Astemizole	5.23	+

Figure 2. Concentration dependence of drug binding in HEK293 cells. Binding was measured over a concentration range covering the expected intracellular total-drug concentrations after incubation with 0.1 μM extracellular drug. Negatively charged compounds are represented by triangles, neutral compounds by circles, and positively charged compounds by squares. Compounds with low lipophilicity (log $D_{7.4} \leq 0$) are represented in white, compounds with intermediate lipophilicity (log $D_{7.4}$: 1−3) in gray, and compounds with high lipophilicity (log $D_{7.4} > 3$) in black. Data are presented as the mean ± SEM.

absence of functional drug transport proteins. Nine of the compounds were predicted to be predominantly uncharged at pH 7.4, 13 as being negatively charged, 7 positively charged, and one compound as being zwitterionic. The ranges and mean values of log P and molecular weight were similar for the different charge groups (Table 1; $p > 0.8$ and $p > 0.5$, respectively), whereas, as expected, the average log $D_{7.4}$ was lower for the charged compounds than for the neutral ones (Table 1; $p = 0.05$). The polar surface area (PSA) was, on average, lower for the positively charged compounds than for the uncharged and negatively charged ones (Table 1; $p = 0.06$).

Concentration Dependence of Drug Binding in HEK293 Cells. A prerequisite for using a single $f_{u,cell}$ value to predict the intracellular accumulation of unbound drug is that the binding is not saturable in the relevant concentration range. To establish the concentration dependence of intracellular binding, we measured $f_{u,cell}$ for a subset of nine physicochemically diverse compounds at five concentrations between 0.01 and 100 μM (this covers the range of total intracellular concentrations expected after incubation with 100 nM extracellular drug, based on preliminary experiments in mock transfected HEK293 cells; data not shown). The subset included compounds with diverse charge and lipophilicity, both of which are molecular characteristics known to affect drug binding in other systems.[5,30]

The results indicate that $f_{u,cell}$ is concentration-independent within the range examined (Figure 2; $p > 0.2$−0.7 depending on the compound). This supports the use of $f_{u,cell}$ measurements at a single concentration in this study to predict intracellular unbound drug concentrations. On the basis of this finding we used a concentration of 0.1 μM for the complete compound set in subsequent measurements of binding and cell uptake.

Molecular Determinants of Intracellular Drug Binding. Measurements of cellular drug binding ($f_{u,cell}$) for the complete compound set covered more than 3 orders of magnitude, ranging from 0.0004 (for nelfinavir) to 0.74 (for caffeine) (Table 2). The majority of the compounds (25 of 30) had unbound fractions below 10%, of which five were below 1% (nelfinavir, astemizole, saquinavir, lovastatin, and lopinavir). No statistically significant differences were observed in $f_{u,cell}$ for compounds from the negative, positive, and neutral charge classes ($p > 0.5$). However, the compounds carrying negative charges at pH 7.4 covered a smaller range of binding values ($f_{u,cell}$ = 0.016−0.31; i.e., 19-fold) compared to the positively charged (0.001−0.61; 420-fold) and neutral compounds (0.0004−0.74; 1730-fold).

As previously observed for liver microsomes[30] and rat hepatocytes,[5,6] binding to cultured HEK293 cells increased with increasing compound lipophilicity. The values of $f_{u,cell}$ can only be between 0 and 1. Thus for modeling purposes, binding was expressed as the ratio of unbound-to-bound drug concentrations (C_u/C_b; which can take on any real number) instead. The linear relationship between log C_u/C_b and lipophilicity (log $D_{7.4}$) gave an r^2 of 0.67 and an average fold error of 2.7 in predictions of binding (Figure 3A). Notably, predictions based on lipophilicity alone overpredicted binding of predominantly unbound compounds and underpredicted that of highly bound compounds.

To improve predictions of cellular drug binding, we developed a multivariate structure-binding relationship using partial least-squares projection (Figure 3B). With this approach, the correlation was improved to $r^2 = 0.90$, with predictions deviating from the measured values by 1.7-fold on average. As expected, the model is dominated by lipophilicity (log $D_{7.4}$ and log P), with higher binding observed for the more lipophilic compounds in the data set (Figure 3C; Table S4). In addition, negative charge (mean electrotopological state; net negative charge at pH 7.4) and aromaticity are among the most influential descriptors in the model; they are associated with decreased binding. Also, several descriptors of molecular shape (medium radius of encompassing ellipsoid; displacement between geometrical and mass center; geometrical length-to-breadth ratio; and the maximum mass-centered molecular radius) collectively indicate that binding is higher for compounds that are stretched out in two dimensions (i.e., having a large surface of interaction) than for molecules with elongated, rod-like shapes.

Comparison to Binding in Other Systems. We were interested in seeing to what extent drug binding in a simplistic cell line reflects that in other systems of varying complexity (Table S2). We first compared binding in the HEK293 cells to literature data for plasma protein binding ($f_{u,plasma}$), a parameter routinely measured in early drug development stages. Considerable deviations were observed in the log−log relationship (Figure 4A; $r^2 = 0.42$). In particular, compounds that were highly bound in either cells or plasma were bound to a smaller extent in the other system, suggesting differences in the binding

dx.doi.org/10.1021/mp4000822 | Mol. Pharmaceutics 2013, 10, 2467−2478

Table 2. Cell Binding, Intracellular Accumulation, and Physicochemical Properties of the Studied Compounds[a]

compound	$pK_{a,acid}$[b]	$pK_{a,base}$[b]	log $D_{7.4}$[b]	$f_{u,cell}$	Kp	Kp_{uu} (observed)[c]	Kp_{uu} (predicted)[d]
Negatively Charged at pH 7.4							
atorvastatin	4.7		2.18	0.022 ± 0.001	2.5 ± 0.1	0.057 ± 0.003	0.5
candesartan	3.7		−0.64	0.075 ± 0.027	1.6 ± 0.2	0.12 ± 0.05	0.5
cerivastatin	4.4	6.6	2.15	0.022 ± 0.003	35 ± 3	0.75 ± 0.12	0.56
diclofenac	4.0		1.56	0.11 ± 0.04	37 ± 6	4.2 ± 1.7	0.5
enalapril	3.2	6.2	−0.61	0.31 ± 0.12	0.52 ± 0.05	0.16 ± 0.06	0.53
fluvastatin	4.7		0.96	0.019 ± 0.004	49 ± 6	0.93 ± 0.22	0.5
indomethacin	4.1		0.74	0.098 ± 0.033	14 ± 2	1.4 ± 0.5	0.5
olmesartan	4.5		1.09	0.041 ± 0.005	0.69 ± 0.09	0.028 ± 0.005	0.5
pitavastatin	4.3	6.0	1.86	0.028 ± 0.008	4.3 ± 0.3	0.12 ± 0.04	0.52
pravastatin	4.9		0.02	0.087 ± 0.021	0.68 ± 0.10	0.059 ± 0.017	0.5
repaglinide	4.3	5.4	3.22	0.016 ± 0.001	72 ± 8	1.1 ± 0.2	0.5
rosiglitazone	3.6		3.10	0.051 ± 0.001	17 ± 2	0.87 ± 0.09	0.5
simvastatin acid	4.9		1.74	0.017 ± 0.0002	42 ± 5	0.70 ± 0.09	0.5
Neutral at pH 7.4							
caffeine			−0.11	0.74 ± 0.20	0.74 ± 0.15	0.54 ± 0.18	1
ketoconazole		5.7	3.91	0.011 ± 0.0001	228 ± 45	2.6 ± 0.5	1.1
lopinavir			4.20	0.0067 ± 0.0001	55 ± 4	0.37 ± 0.03	1
lovastatin			4.49	0.0032 ± 0.0002	440 ± 64	1.4 ± 0.2	1
nelfinavir	9.7	5.7	4.71	0.00043 ± 0.00004	424 ± 113	0.18 ± 0.05	1.1
ondansetron		6.8	2.05	0.11 ± 0.02	24 ± 3	2.7 ± 0.7	1.9
prazosin		6.6	1.18	0.057 ± 0.007	27 ± 6	1.6 ± 0.4	1.6
ritonavir			4.56	0.016 ± 0.002	103 ± 13	1.7 ± 0.3	1
saquinavir		5.6	4.16	0.0024 ± 0.0003	259 ± 56	0.62 ± 0.16	1.1
Positively Charged at pH 7.4							
astemizole		8.0	5.23	0.0014 ± 0.0002	268 ± 31	0.38 ± 0.08	4.4
diltiazem		7.9	2.93	0.060 ± 0.013	50 ± 9	3.0 ± 0.9	4.2
imipramine		9.0	3.26	0.017 ± 0.003	425 ± 96	7.1 ± 2.0	5.1
irinotecan		8.7	2.57	0.030 ± 0.005	8.7 ± 0.8	0.26 ± 0.05	5
metoprolol		9.4	0.05	0.61 ± 0.23	12 ± 1	7.3 ± 2.8	5.2
propranolol		9.3	1.17	0.035 ± 0.005	138 ± 15	4.8 ± 0.8	5.2
verapamil		8.1	3.86	0.034 ± 0.003	151 ± 32	5.1 ± 1.2	4.5
Zwitterion at pH 7.4							
fexofenadine	4.5	8.8	3.00	0.058 ± 0.008	1.7 ± 0.2	0.099 ± 0.019	0.99
min	3.2	5.4	−0.64	0.00043	0.52	0.028	0.5
max	9.7	9.4	5.23	0.74	440	7.3	5.2
mean	4.6	7.3	2.29	0.090	96	1.7	1.7
SEM	0.4	0.3	0.31	0.031	25	0.4	0.3

[a]Compounds were divided into their charge groups on the basis of the most abundant charge species at pH 7.4. Data are presented as the mean ± SEM. [b]Predicted using ADMET predictor (Simulations Plus, Lancaster, CA). [c]The Kp_{uu} value measured in mock-transfected ("transporter silent") HEK293 cells refers to a "passive" Kp_{uu} value, that does not include active transport mechanisms that can influence accumulation in other cell types. [d]Predicted using the equilibrium pH partitioning model (eq 6).

interactions. Such differences are expected, considering that binding in plasma primarily describes drug interactions with albumin and other proteins, whereas the HEK293 homogenate is a mixture of all cell contents including proteins, DNA, and membrane lipids. The correlation did not improve when applying a recently proposed equation for transforming plasma to hepatocyte binding (r^2 = 0.40; data not shown),[31] and it improved only slightly for binding to whole blood (calculated from $f_{u,plasma}$ and the blood-to-plasma total concentration ratio, assuming equal unbound concentrations in blood cells and plasma; r^2 = 0.57). Next, we compared binding in HEK293 cells to that in liver-cell derived systems. Hepatic microsomes, being a purified fraction of liver homogenate that contains both proteins and lipid membranes, are expected to more closely resemble the HEK293 cells. Accordingly, a relatively strong correlation was observed between unbound fractions in HEK293 cells and those reported in microsomes ($f_{u,microsome}$) (r^2 = 0.77; data not shown). Importantly, microsomal binding is known to depend on the concentration of microsomes in the incubation.[30,32] Using eq 2 to account for the dilution that occurs when preparing microsomes from hepatocytes (based on physiologically relevant values of microsomal content; 47 mg microsomal protein/g rat liver and 32 mg microsomal protein/g human liver), this correlation was further improved (Figure 4B; r^2 = 0.88). Still, the dilution-corrected microsomal binding was, on average, 6.2-fold higher than in the HEK293 cells, suggesting more extensive binding in hepatocyte-derived systems than in HEK293 cells.

dx.doi.org/10.1021/mp4000822 | Mol. Pharmaceutics 2013, 10, 2467−2478

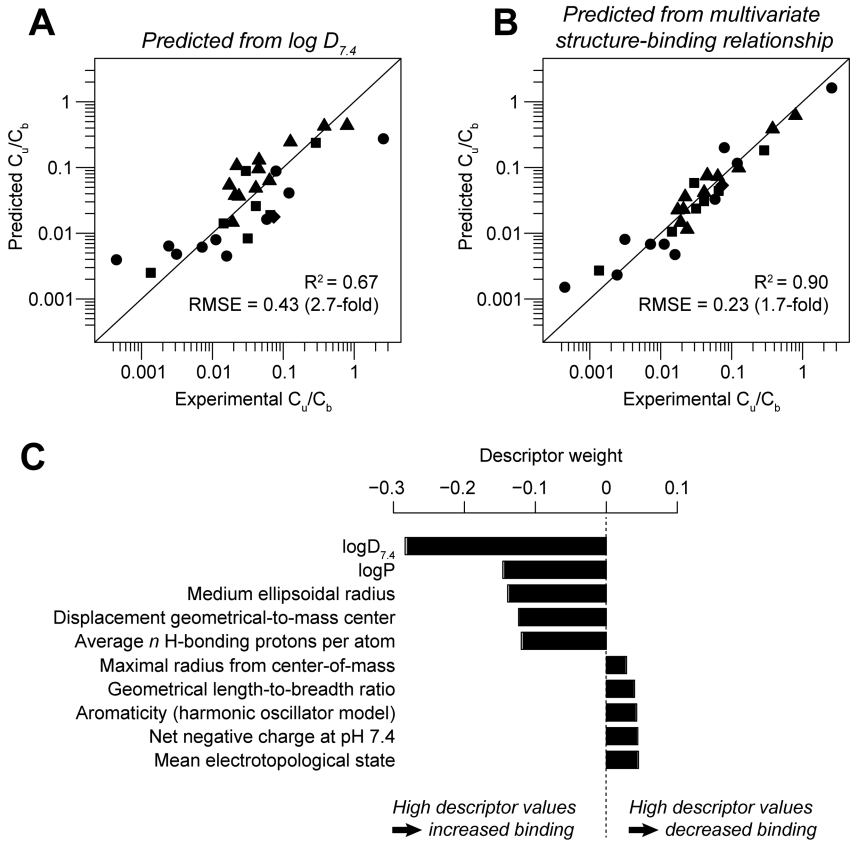

Figure 3. Predictions of intracellular drug binding from molecular properties. Drug binding is represented as the ratio of unbound-to-bound drug concentrations (C_u/C_b). (A) Prediction of drug binding from lipophilicity (log $D_{7.4}$) using linear regression. (B) Predictions from a multivariate structure-binding relationship using partial least-squares projection. In A and B, negatively charged compounds are represented by triangles, neutral compounds by circles, and positively charged compounds by squares. (C) The most influential descriptors in the multivariate model were related to lipophilicity (log $D_{7.4}$, log P), charge (mean electrotopological state, net negative charge, average number of hydrogen bonding protons), aromaticity (harmonic oscillator model), and shape (medium ellipsoidal radius, displacement of geometrical-to-mass center, maximal radius from center-of-mass, geometrical length-to-breadth ratio). Descriptors with negative coefficients had higher values in extensively bound compounds, and descriptors with positive coefficients had higher values in compounds with low binding.

To further explore such binding differences between cell types, we applied the homogenate dialysis technique to measure binding in cryopreserved human hepatocytes. A similar correlation was obtained as for the corrected microsomal binding (Figure 4C; r^2 = 0.91), with 4.9-fold higher binding on average in human hepatocytes than in the HEK293 cells. These cell type-specific differences in binding were further corroborated by data obtained in rat hepatocytes using previously reported methods (Table S2).[10−12] The binding in rat hepatocytes was, on average, 3.7-fold more extensive, yet it strongly correlated with binding in the HEK293 cell line (Figure 4D; r^2 = 0.84). In contrast, mechanistic modeling of drug uptake in rat hepatocytes[5,6] suggested a 2.7-fold lower extent of binding than what we observed in HEK293 cells and 10-fold lower than that in hepatocytes (n = 9) (data not shown). The noted difficulty of fitting the intracellular binding and passive permeability components simultaneously[5,6]—since these are strongly correlated—may contribute to the differences observed between modeling-derived and experimentally determined binding estimates. We propose that experimental binding measurements can guide future modeling efforts to better parameter estimates and improved model fits.

Accumulation of Total and Unbound Drug in HEK293 Cells. Toward our overall goal of measuring intracellular unbound drug levels (Figure 1), we measured the steady-state accumulation of total drug in intact HEK293 cells (Kp; Table 2) in parallel with the measurements of intracellular drug binding described above (Measurements of Intracellular Drug Binding section). Kp correlated with molecular charge, increasing from 7 ± 6 (range: 0.5−72) for the negatively charged compounds, to 47 ± 8 (range: 0.7−440) for the neutrals, and 74 ± 4 (range: 8.8−420) for the compounds with a positive charge at pH 7.4. In addition, the increase in the lipophilicity of compounds with the same charge led to an increase in the ratio between the total intracellular and medium concentrations (Kp).

By compensating the measurements of total drug accumulation (Kp) for the intracellular binding ($f_{u,cell}$), we then calculated the accumulation ratio for unbound drug (Kp_{uu}) for each compound (eq 4). In comparison with the accumulation ratios based on total drug concentrations (which include effects from both the accumulation of unbound drug and the intracellular binding), the Kp_{uu} covered a more narrow range (26-fold compared to 850-fold difference for Kp between the highest and the lowest value).

For passively diffusing compounds, an equilibrium Kp_{uu} of 1 is expected, meaning that the unbound drug concentrations are the same in the extracellular and intracellular compartments. This expectation was supported by the experimental results, with a mean Kp_{uu} of 1.2 ± 0.3 (median 1.0) for the uncharged

dx.doi.org/10.1021/mp4000822 | Mol. Pharmaceutics 2013, 10, 2467−2478

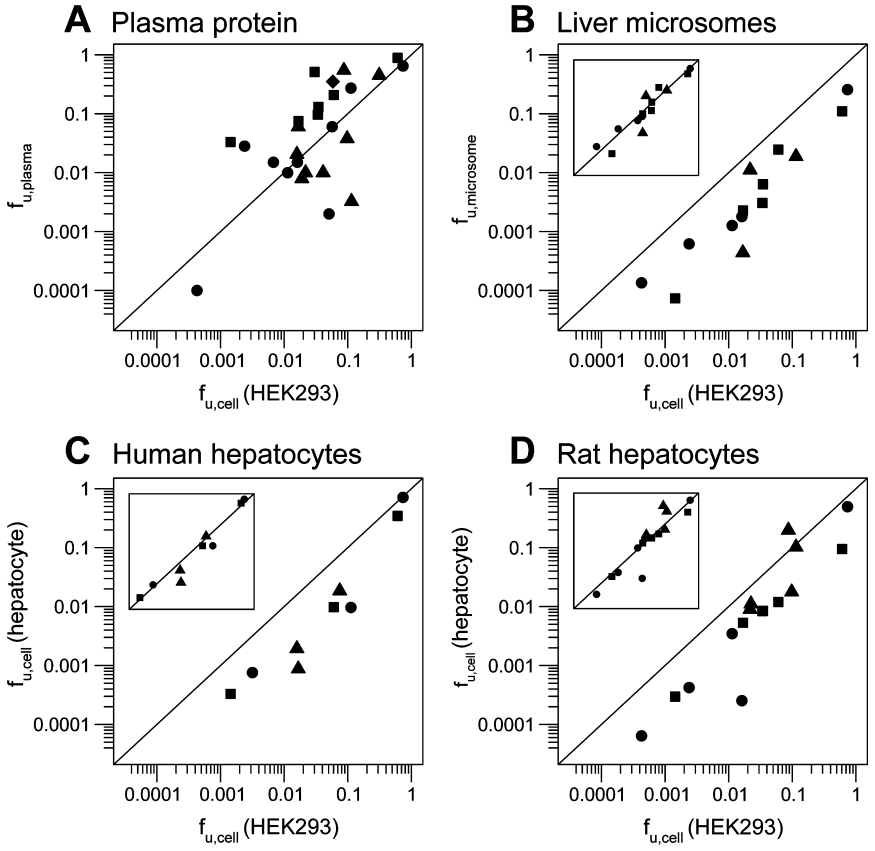

Figure 4. Relationship between drug binding in HEK293 cells and other cell types and experimental systems. Binding in HEK293 cells is compared to plasma protein binding (A); binding in liver microsomes (B; accounting for the dilution that occurs in the preparation of microsomes from liver tissue); human hepatocytes (C; measured using the methodology developed in this paper); and rat hepatocytes (D; derived from cellular uptake studies and assuming that drug accumulation is not affected by active transport mechanisms or metabolism). Inserts show the corresponding correlations obtained after accounting for different binding capacities in the compared systems, using least-squares optimization of eq 2 (resulting in relative dilution factors of 6.2, 4.9, and 3.7 in B, C, and D, respectively). Data on binding to plasma protein, liver microsomes, and rat hepatocytes were collated from the literature (Table S2). Negatively charged compounds are represented by triangles, neutral compounds by circles, and positively charged compounds by squares. Lines represent equal binding in the two systems.

compounds. For the negatively charged compounds, the mean Kp_{uu} was slightly lower (0.8 ± 0.3; median 0.7), while a higher mean Kp_{uu} was observed for the positively ionizable compounds (4.0 ± 1.1; median 4.8) (Figure 5A). The higher value for the positively charged compounds is consistent with the trapping of charged species in acidic subcellular compartments such as endosomes and lysosomes (collectively "endolysosomes"),[33−35] and the lower-than-unity value for acids is expected from the pH gradient across the plasma membrane (pH 7.4 in the extracellular medium and 7.1 in the cytosol of HEK293 cells[26]). Due to the negligible expression of transport proteins and drug-metabolizing enzymes in HEK293 cells,[13] pH-dependent subcellular partitioning is expected to be the major determinant of equilibrium Kp_{uu}.

To further explore whether the experimental data supported this expectation, we built a three-compartment model of subcellular equilibrium partitioning (consisting of medium, cytosolic, and endolysosomal compartments; eq 6).[34,35] On average, the observed Kp_{uu} for each charge category followed those predicted by the model. However, as has been observed previously for drug distribution in the brain,[35] the equilibrium was also affected by additional mechanisms, leading to variability within each charge category. For example, in our study the negatively charged compounds separated into two clusters with average Kp_{uu} close to 1 and 0.1, respectively, compared to the predicted value of ∼0.5 for acids with a pK_a < 5. The two clusters have similar $f_{u,cell}$ and log $D_{7.4}$ (p > 0.3 and p > 0.2, respectively) but differ in the Kp and polar surface area (p = 0.002 and p = 0.035, respectively), suggesting that limited permeability could contribute to the observed lower Kp_{uu} of some compounds. However, this was not reflected in a markedly longer time to equilibrium for prototypical compounds from this cluster (e.g., candesartan reached equilibrium after 10 min incubation; data not shown).

To confirm the impact of endolysosomal trapping on the unbound accumulation ratio, chloroquine was used to increase the lysosomal pH.[18] Cellular uptake was measured for six compounds (three weak acids and three weak bases) in the presence of chloroquine, and the Kp_{uu} was calculated (eq 4). As expected, increasing chloroquine concentrations did not affect the Kp_{uu} of the negatively charged compounds (diclofenac, indomethacin, and simvastatin acid; Figure 5C), whereas a strong, concentration-dependent decrease in the Kp_{uu} was observed for the positively charged compounds (diltiazem, propranolol, and verapamil; Figure 5D). A chloroquine concentration of 1 μM is expected to increase the lysosomal pH by 0.5 units (with an increase of another 0.5 units for each 10-fold increase in chloroquine concentration[18]). This allowed us to obtain an approximate estimate of the pH of the endolysosomal space at the tested chloroquine concentrations

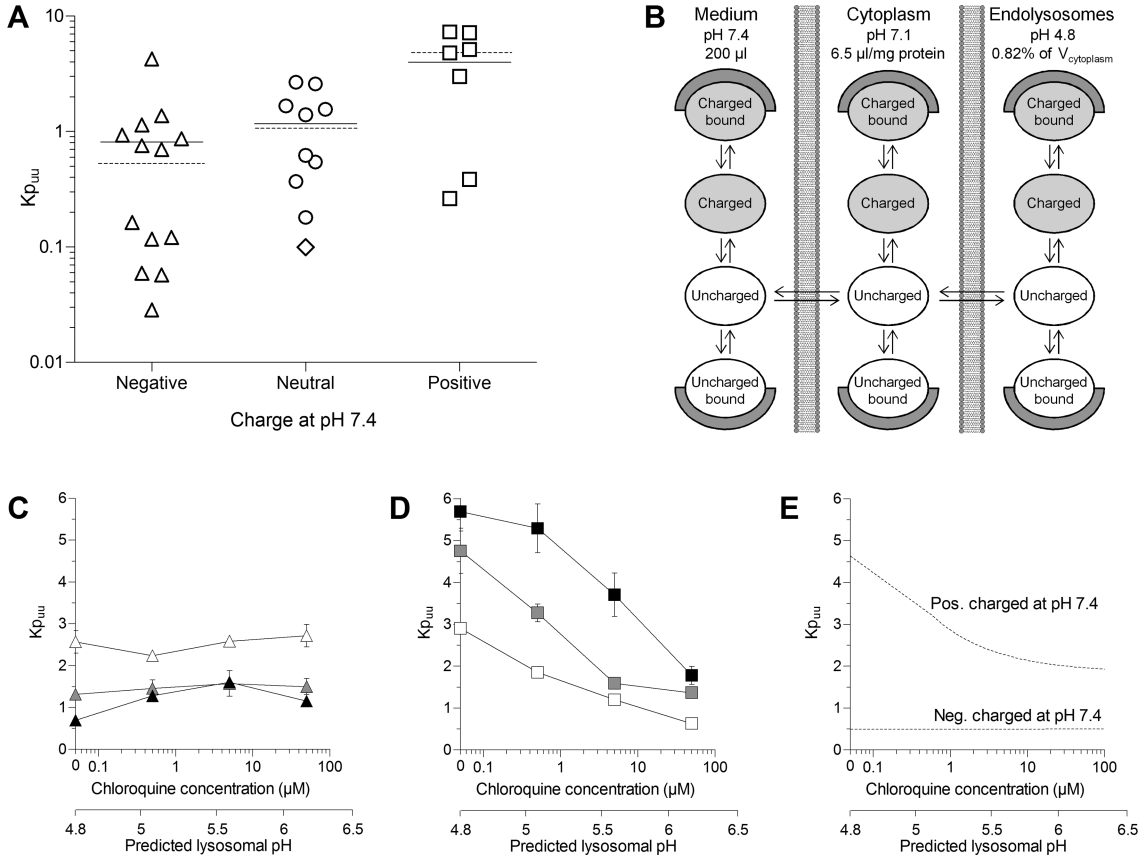

Figure 5. Impact of molecular charge on subcellular drug distribution. (A) Influence of charge on the unbound drug-accumulation ratio (Kp_{uu}). Negatively charged compounds are represented by triangles, neutral compounds by circles, and positively charged compounds by squares. The solid lines represent the mean, and the dashed lines represent the predictions from the model of equilibrium subcellular partitioning shown in panel B. (B) Schematic drawing of the equilibria included in the subcellular partitioning model. At equilibrium, the concentration of unbound and uncharged drug is equal in each of the three modeled compartments (extracellular medium, cytoplasm, and acidic cellular compartments, termed "endolysosomes"). The pH in each compartment determines the subcellular equilibria between uncharged and charged molecular species. (C–D) The effect of chloroquine on the Kp_{uu} of acidic (C; white, diclofenac; gray, indomethacin; black, simvastatin acid) and basic drugs (D; white, diltiazem; gray, propranolol; black, verapamil). Neutralization of the pH gradient between cytoplasm and endolysosomal compartments does not affect the cellular accumulation of acids but reduces the accumulation of basic drugs. (E) Expected effects on the Kp_{uu} of acidic and basic drugs predicted using the three-compartment equilibrium partitioning model. The endolysosomal pH expected at different chloroquine concentrations were predicted based on the relationship in Poole and Ohkuma.[18]

and to predict the Kp_{uu} of the tested compounds in the three-compartment cell model (according to the Modeling of pH-Dependent Unbound Drug Accumulation section). The predictions are in line with our results, with no change of Kp_{uu} for the negatively charged compounds and a decrease for the positively charged compounds (Figure 5E).

DISCUSSION

Unbound drug concentrations inside the cell determine their intracellular pharmacology, toxicology, and disposition, and yet this parameter has largely been ignored in drug discovery, probably due to measurement difficulties. Here, we present a new technique combining measurements of binding to cell homogenates and steady-state uptake in living cells, which allows rapid determination of unbound drug concentrations on a small scale (Figure 1). The method expands on previous work in tissue homogenates,[36,37] adding the advantage of measurements in highly controlled cell cultures. This allows detailed studies of intracellular drug accumulation in defined cell types, in which specific drug transport, metabolism, or target pathways can be selectively introduced or inhibited.[38]

Binding in HEK293 cells (which lack functional drug transporters and drug metabolizing enzymes) was strongly correlated with compound lipophilicity, with the more lipophilic compounds being bound to a larger extent to cellular structures; similar observations have been reported for rat hepatocytes.[5,6] In addition, other physicochemical characteristics of the compounds appear to influence $f_{u,cell}$. Among these, a negative molecular charge and the presence of aromatic substructures both decreased cellular binding, whereas larger molecular surface areas resulted in more extensive binding (Figure 3). The importance of these physicochemical properties, together with the fact that the binding process was not saturable with increasing compound concentration (up to 100 μM; Figure 2), suggest that cellular binding may be driven primarily by partitioning to cellular membranes. This hypothesis is in line with both the increased binding observed with increasing log $D_{7.4}$ (describing compound affinity for membrane lipids) and the decreased binding that resulted from negative molecular charge and aromaticity (possibly linked to electrostatic repulsion between negatively charged lipids and electron-rich functional groups in the drug molecules). In

dx.doi.org/10.1021/mp4000822 | Mol. Pharmaceutics 2013, 10, 2467–2478

addition, the demonstrated importance of lipid content for the tissue partitioning of drugs further supports this hypothesis.[39]

Binding in HEK293 cells was poorly correlated with binding in plasma (Figure 4A). It could be expected that binding in plasma does not adequately reflect binding in the more complex cell environment. Plasma binding is mainly driven by interactions with proteins,[40] whereas in cellular binding we expect membrane partitioning to play an important role. The weak correlation clearly suggests that plasma binding is not a suitable surrogate for cellular drug binding. In contrast, the much stronger correlation between binding in HEK293 cells and other cell types, such as hepatocytes, raises the possibility of using simple cell lines as surrogates for binding in more complex, primary human cells. Importantly, such applications would require correction factors since our results suggest that HEK293 cells contain approximately 4- to 6-fold lower concentrations of binding components than human and rat hepatocytes (Figure 4B–D). Based on differences between their respective tissues of origin, hepatocytes (being the major cell type in liver tissue) are expected to contain higher levels of lipids and protein than the HEK293 cells (which originate from human embryonic kidney): for example, lipid and protein contents are 2- to 2.5-fold higher in liver tissue than in the fetal kidney.[41]

Combining cellular binding and uptake experiments allowed us to determine the unbound accumulation ratio Kp_{uu}, which in the HEK293 cells (that lack significant drug metabolism and active drug transport) is expected to be independent of the concentration of the compounds. Due to differences in pH among the medium, cytosolic, and endolysosomal compartments, this parameter is not always equal to 1 (Figure 5), as has been assumed in some reports.[5−7] In fact, using a mathematical model of these three compartments, we showed that such pH differences can contribute to a theoretical 10-fold range in Kp_{uu} between acidic (pK_a < 5) and basic (pK_a > 9) compounds, due to subcellular charge trapping.[33]

The model predictions were consistent with our experimentally determined Kp_{uu} values, and the impact of charge trapping on the differences between acids and bases was further substantiated by Kp_{uu} measurements in the presence of chloroquine, which increases lysosomal pH.[18] The model predicted that the acidic compounds would be mainly affected by the cytosol:medium pH difference, which leads to higher ionized fractions in the medium. Due to the limited permeability of the charged species, this is expected to contribute to a cytosol-to-medium ratio of unbound concentrations of 0.5, with virtually no distribution to the endolysosomal compartment. For that reason, it is not surprising that chloroquine-induced increases in lysosomal pH had no effect on the intracellular accumulation of the acids. In contrast, basic compounds will be affected by both the cytosol:medium and endolysosomal:cytosol pH differences. These would result in unbound concentration ratios of 2 and >200 across the respective membranes, since the transmembrane pH gradients will lead to higher ionized fractions (and entrapment) of the basic drugs in the more acidic (i.e., endolysosomal) compartments. Because of the low volumes of the endolysosomal compartments, these ratios combine to an overall intracellular-to-medium Kp_{uu} of approximately 5-fold. Consequently, any increase in endolysosomal pH, such as the one triggered by chloroquine, would have a major impact on the intracellular distribution of basic compounds. Notably, the mathematical model is a simplification of the subcellular drug distribution process, where some compounds may partition to other organelles (e.g., mitochondria)[42] or induce changes in the lysosomes (e.g., increase in pH or volume).[43] In addition, the model assumes that all compounds are rapidly distributed across cellular membranes and reach an equilibrium based solely on charge-driven sequestration. These simplifications might explain some discrepancies between the model predictions and the experimental results seen for highly polar compounds, for which membrane permeability may be limited.

In conclusion, we show that our method is applicable to measurements of drug binding and unbound drug accumulation in cultured cells. When applied to a model cell line that lacks functional transporters and drug-metabolizing enzymes, drug binding was predictive of binding in hepatocytes and hepatic microsomes. Similarly, the intracellular unbound drug accumulation was consistent with passive, pH-dependent subcellular partitioning. As the method uses parallel measurements of drug binding and accumulation to derive unbound intracellular concentrations, the assumptions of negligible metabolic clearance and strictly passive distribution that hamper most alternative techniques are eliminated. Our methodology is thus readily applicable to more complex systems such as primary cells from animal or human tissue, or cell lines with controlled expression of transporters and metabolic enzymes. In ongoing experiments to be published separately, we apply this approach to assess the impact of transport proteins on intracellular unbound drug concentrations and activity.

■ ASSOCIATED CONTENT

Supporting Information

UPLC-MS/MS methods; measurements of binding in other experimental systems; list of molecular descriptors used for structure-binding model; list of nonscaled coefficients of descriptors depicted in Figure 3C. This material is available free of charge via the Internet at http://pubs.acs.org.

■ AUTHOR INFORMATION

Corresponding Author

*E-mail: per.artursson@farmaci.uu.se; telephone: +46-18 471 44 71; fax: +46 18 471 42 23.

Notes

The authors declare no competing financial interest.

■ ACKNOWLEDGMENTS

The authors gratefully acknowledge SimulationsPlus for access to the ADMET Predictor software. The authors also acknowledge the support from Science for Life Laboratory (SciLifeLab). This work was supported by the Swedish Fund for Research Without Animal Experiments, Magn. Bergvalls Stiftelse, and the Swedish Research Council (grants nos. 9478 and 21386). A.M. was supported by a Ph.D. training grant from Fundação para a Ciência e Tecnologia (grant no. SFRH/BD/68304/2010).

■ ABBREVIATIONS

HEK293, human embryonic kidney 293 cells; DMEM, Dulbecco's modified Eagle's medium; FBS, fetal bovine serum; HBSS, Hank's buffered salt solution; DMSO, dimethyl sulfoxide; PBS, phosphate-buffered saline; Kp, ratio between total compound concentrations in the cells and in the medium; $f_{u,cell}$, fraction unbound in HEK293 cells; Kp_{uu}, ratio between unbound compound concentrations in the cells and in the

medium; SMILES, simplified molecular-input line-entry system; ADME, absorption, distribution, metabolism, and excretion; PLS, partial least-squares; RMSE, root-mean-squared error of prediction; PSA, polar surface area

REFERENCES

(1) Overington, J. P.; Al-Lazikani, B.; Hopkins, A. L. How many drug targets are there? *Nat. Rev. Drug Discovery* **2006**, *5* (12), 993−6.

(2) Pang, K. S.; Rowland, M. Hepatic clearance of drugs. I. Theoretical considerations of a "well-stirred" model and a "parallel tube" model. Influence of hepatic blood flow, plasma and blood cell binding, and the hepatocellular enzymatic activity on hepatic drug clearance. *J. Pharmacokinet. Biopharm.* **1977**, *5* (6), 625−53.

(3) Hallifax, D.; Foster, J. A.; Houston, J. B. Prediction of human metabolic clearance from in vitro systems: retrospective analysis and prospective view. *Pharm. Res.* **2010**, *27* (10), 2150−61.

(4) Paine, S. W.; Parker, A. J.; Gardiner, P.; Webborn, P. J.; Riley, R. J. Prediction of the pharmacokinetics of atorvastatin, cerivastatin, and indomethacin using kinetic models applied to isolated rat hepatocytes. *Drug Metab. Dispos.* **2008**, *36* (7), 1365−74.

(5) Yabe, Y.; Galetin, A.; Houston, J. B. Kinetic characterization of rat hepatic uptake of 16 actively transported drugs. *Drug Metab. Dispos.* **2011**, *39* (10), 1808−14.

(6) Ménochet, K.; Kenworthy, K. E.; Houston, J. B.; Galetin, A. Simultaneous assessment of uptake and metabolism in rat hepatocytes: a comprehensive mechanistic model. *J. Pharmacol. Exp. Ther.* **2012**, *341* (1), 2−15.

(7) Ménochet, K.; Kenworthy, K. E.; Houston, J. B.; Galetin, A. Use of Mechanistic Modelling to Assess Inter-Individual Variability and Inter-species Differences in Active Uptake in Human and Rat Hepatocytes. *Drug Metab. Dispos.* **2012**, *40*, 1744−56.

(8) Yamazaki, M.; Suzuki, H.; Hanano, M.; Tokui, T.; Komai, T.; Sugiyama, Y. Na(+)-independent multispecific anion transporter mediates active transport of pravastatin into rat liver. *Am. J. Physiol.* **1993**, *264* (1 Pt 1), G36−44.

(9) Yamano, K.; Yamamoto, K.; Kotaki, H.; Takedomi, S.; Matsuo, H.; Sawada, Y.; Iga, T. Correlation between in vivo and in vitro hepatic uptake of metabolic inhibitors of cytochrome P-450 in rats. *Drug Metab. Dispos.* **1999**, *27* (11), 1225−31.

(10) Hallifax, D.; Houston, J. B. Uptake and intracellular binding of lipophilic amine drugs by isolated rat hepatocytes and implications for prediction of in vivo metabolic clearance. *Drug Metab. Dispos.* **2006**, *34* (11), 1829−36.

(11) Kilford, P. J.; Gertz, M.; Houston, J. B.; Galetin, A. Hepatocellular binding of drugs: correction for unbound fraction in hepatocyte incubations using microsomal binding or drug lipophilicity data. *Drug Metab. Dispos.* **2008**, *36* (7), 1194−7.

(12) Austin, R. P.; Barton, P.; Mohmed, S.; Riley, R. J. The binding of drugs to hepatocytes and its relationship to physicochemical properties. *Drug Metab. Dispos.* **2005**, *33* (3), 419−25.

(13) Ahlin, G.; Hilgendorf, C.; Karlsson, J.; Szigyarto, C. A.; Uhlen, M.; Artursson, P. Endogenous gene and protein expression of drug-transporting proteins in cell lines routinely used in drug discovery programs. *Drug Metab. Dispos.* **2009**, *37* (12), 2275−83.

(14) Karlgren, M.; Ahlin, G.; Bergström, C. A.; Svensson, R.; Palm, J.; Artursson, P. In Vitro and In Silico Strategies to Identify OATP1B1 Inhibitors and Predict Clinical Drug-Drug Interactions. *Pharm. Res.* **2011**, *29*, 411−26.

(15) Lecluyse, E. L.; Alexandre, E. Isolation and culture of primary hepatocytes from resected human liver tissue. *Methods Mol. Biol.* **2010**, *640*, 57−82.

(16) Alexandre, E.; Viollon-Abadie, C.; David, P.; Gandillet, A.; Coassolo, P.; Heyd, B.; Mantion, G.; Wolf, P.; Bachellier, P.; Jaeck, D.; Richert, L. Cryopreservation of adult human hepatocytes obtained from resected liver biopsies. *Cryobiology* **2002**, *44* (2), 103−13.

(17) Kalvass, J. C.; Maurer, T. S. Influence of nonspecific brain and plasma binding on CNS exposure: implications for rational drug discovery. *Biopharm. Drug. Dispos.* **2002**, *23* (8), 327−38.

(18) Poole, B.; Ohkuma, S. Effect of weak bases on the intralysosomal pH in mouse peritoneal macrophages. *J. Cell Biol.* **1981**, *90* (3), 665−9.

(19) Gillen, C. M.; Forbush, B. Functional interaction of the K-Cl cotransporter (KCC1) with the Na-K-Cl cotransporter in HEK-293 cells. *Am. J. Physiol., Cell Physiol.* **1999**, *276* (2), C328−C336.

(20) Fagerberg, J. H.; Tsinman, O.; Sun, N.; Tsinman, K.; Avdeef, A.; Bergström, C. A. Dissolution Rate and Apparent Solubility of Poorly Soluble Drugs in Biorelevant Dissolution Media. *Mol. Pharmaceutics* **2010**, *7*, 1419−30.

(21) Matsson, P.; Pedersen, J. M.; Norinder, U.; Bergström, C. A.; Artursson, P. Identification of novel specific and general inhibitors of the three major human ATP-binding cassette transporters P-gp, BCRP and MRP2 among registered drugs. *Pharm. Res.* **2009**, *26* (8), 1816−31.

(22) Matsson, P.; Bergström, C. A.; Nagahara, N.; Tavelin, S.; Norinder, U.; Artursson, P. Exploring the role of different drug transport routes in permeability screening. *J. Med. Chem.* **2005**, *48* (2), 604−13.

(23) Kido, Y.; Matsson, P.; Giacomini, K. M. Profiling of a prescription drug library for potential renal drug-drug interactions mediated by the organic cation transporter 2. *J. Med. Chem.* **2011**, *54* (13), 4548−58.

(24) Freyhult, E.; Prusis, P.; Lapinsh, M.; Wikberg, J. E.; Moulton, V.; Gustafsson, M. G. Unbiased descriptor and parameter selection confirms the potential of proteochemometric modelling. *BMC Bioinformatics* **2005**, *6*, 50.

(25) Shore, P. A.; Brodie, B. B.; Hogben, C. A. The gastric secretion of drugs: a pH partition hypothesis. *J. Pharmacol. Exp. Ther.* **1957**, *119* (3), 361−9.

(26) Amlal, H.; Wang, Z.; Burnham, C.; Soleimani, M. Functional Characterization of a Cloned Human Kidney Na^+:HCO_3^- Cotransporter. *J. Biol. Chem.* **1998**, *273* (27), 16810−16815.

(27) Reeves, D. C.; Liebelt, D. A.; Lakshmanan, V.; Roepe, P. D.; Fidock, D. A.; Akabas, M. H. Chloroquine-resistant isoforms of the Plasmodium falciparum chloroquine resistance transporter acidify lysosomal pH in HEK293 cells more than chloroquine-sensitive isoforms. *Mol. Biochem. Parasitol.* **2006**, *150* (2), 288−299.

(28) Weibel, E. R.; Stäubli, W.; Gnägi, H. R.; Hess, F. A. Correlated morphometric and biochemical studies on the liver cell. *J. Cell Biol.* **1969**, *42* (1), 68−91.

(29) Niemi, M.; Pasanen, M. K.; Neuvonen, P. J. Organic anion transporting polypeptide 1B1: a genetically polymorphic transporter of major importance for hepatic drug uptake. *Pharmacol. Rev.* **2011**, *63* (1), 157−81.

(30) Austin, R. P.; Barton, P.; Cockroft, S. L.; Wenlock, M. C.; Riley, R. J. The influence of nonspecific microsomal binding on apparent intrinsic clearance, and its prediction from physicochemical properties. *Drug Metab. Dispos.* **2002**, *30* (12), 1497−503.

(31) Jones, H. M.; Barton, H. A.; Lai, Y.; Bi, Y. A.; Kimoto, E.; Kempshall, S.; Tate, S. C.; El-Kattan, A.; Houston, J. B.; Galetin, A.; Fenner, K. S. Mechanistic pharmacokinetic modeling for the prediction of transporter-mediated disposition in humans from sandwich culture human hepatocyte data. *Drug Metab. Dispos.* **2012**, *40* (5), 1007−17.

(32) Margolis, J. M.; Obach, R. S. Impact of nonspecific binding to microsomes and phospholipid on the inhibition of cytochrome P4502D6: implications for relating in vitro inhibition data to in vivo drug interactions. *Drug Metab. Dispos.* **2003**, *31* (5), 606−11.

(33) de Duve, C.; de Barsy, T.; Poole, B.; Trouet, A.; Tulkens, P.; Van Hoof, F. Commentary. Lysosomotropic agents. *Biochem. Pharmacol.* **1974**, *23* (18), 2495−531.

(34) Hallifax, D.; Houston, J. B. Saturable uptake of lipophilic amine drugs into isolated hepatocytes: mechanisms and consequences for quantitative clearance prediction. *Drug Metab. Dispos.* **2007**, *35* (8), 1325−32.

(35) Fridén, M.; Bergström, F.; Wan, H.; Rehngren, M.; Ahlin, G.; Hammarlund-Udenaes, M.; Bredberg, U. Measurement of unbound drug exposure in brain: modeling of pH partitioning explains diverging

results between the brain slice and brain homogenate methods. *Drug Metab. Dispos.* **2011**, *39* (3), 353−62.
(36) Harashima, H.; Sugiyama, Y.; Sawada, Y.; Iga, T.; Hanano, M. Comparison between in-vivo and in-vitro tissue-to-plasma unbound concentration ratios (Kp,f) of quinidine in rats. *J. Pharm. Pharmacol.* **1984**, *36* (5), 340−2.
(37) Fridén, M.; Gupta, A.; Antonsson, M.; Bredberg, U.; Hammarlund-Udenaes, M. In vitro methods for estimating unbound drug concentrations in the brain interstitial and intracellular fluids. *Drug Metab. Dispos.* **2007**, *35* (9), 1711−9.
(38) Karlgren, M.; Vildhede, A.; Norinder, U.; Wisniewski, J. R.; Kimoto, E.; Lai, Y.; Haglund, U.; Artursson, P. Classification of inhibitors of hepatic organic anion transporting polypeptides (OATPs): influence of protein expression on drug-drug interactions. *J. Med. Chem.* **2012**, *55* (10), 4740−63.
(39) Graham, H.; Walker, M.; Jones, O.; Yates, J.; Galetin, A.; Aarons, L. Comparison of in-vivo and in-silico methods used for prediction of tissue: plasma partition coefficients in rat. *J. Pharm. Pharmacol.* **2012**, *64* (3), 383−96.
(40) Smith, D. A.; Di, L.; Kerns, E. H. The effect of plasma protein binding on in vivo efficacy: misconceptions in drug discovery. *Nat. Rev. Drug Discovery* **2010**, *9* (12), 929−39.
(41) White, D. R.; Widdowson, E. M.; Woodard, H. Q.; Dickerson, J. W. The composition of body tissues (II). Fetus to young adult. *Br. J. Radiol.* **1991**, *64* (758), 149−59.
(42) Durazo, S. A.; Kadam, R. S.; Drechsel, D.; Patel, M.; Kompella, U. B. Brain mitochondrial drug delivery: influence of drug physicochemical properties. *Pharm. Res.* **2011**, *28* (11), 2833−47.
(43) Logan, R.; Funk, R. S.; Axcell, E.; Krise, J. P. Drug-drug interactions involving lysosomes: mechanisms and potential clinical implications. *Expert Opin. Drug. Metab. Toxicol.* **2012**, *8* (8), 943−58.